Research Square

Preprints are preliminary reports that have not undergone peer review. They should not be considered conclusive, used to inform clinical practice, or referenced by the media as validated information.

Intraperitoneal thermal priming followed by intravenous liposomal or free cisplatin in a murine ovarian cancer peritoneal dissemination model

Shiyu Zhang
China-Japan Friendship Hospital
Chang Zhou
China-Japan Friendship Hospital
Caiyao Chen
Beijing University of Chemical Technology
Jing Liang
Beijing University of Chemical Technology
Bin Ling
lingbin@zryhyy.com.cn

China-Japan Friendship Hospital

Research Article

Keywords: ovarian cancer, peritoneal dissemination, thermal priming, saline perfusion, liposomal cisplatin, tumor platinum, toxicology

Posted Date: October 22nd, 2026

DOI: https://doi.org/10.21203/rs.3.rs-11099160/v1

License: This work is licensed under a Creative Commons Attribution 4.0 International License. Read Full License

Additional Declarations: No competing interests reported.

Abstract

Background

Regional heating may influence the response to subsequently administered chemotherapy. We evaluated intraperitoneal saline perfusion followed by intravenous liposomal cisplatin in a murine model of ovarian cancer peritoneal dissemination.

Methods

Female mice bearing intraperitoneal ID8-Luc tumors received saline perfusion at nominal temperatures of 37, 41, 43, or 45°C for 15 min after the target intraperitoneal temperature was reached. Free cisplatin or liposomal cisplatin (L-Lip@DDP) was administered at 2 mg/kg cisplatin equivalents by tail-vein injection 30 min after perfusion completion, with treatment three times weekly for 3 weeks. Assessments included formulation characterization, intraperitoneal temperature, optical imaging, tumor platinum content, ascites, representative gross and histological findings, tumor immunohistochemistry, body weight, and serum biochemical markers. Temperature-dependent cellular fluorescence was examined separately in ID8 cells.

Results

Tumor platinum content was higher with L-Lip@DDP than with free cisplatin at each tested temperature. Cellular fluorescent foci were more numerous at 41–45°C than at 37°C and peaked at 43°C. Ascites volumes were lower in the L-Lip@DDP groups, with the lowest plotted volume at 43°C. The 43°C condition also had the highest plotted tumor platinum content, lowest Ki-67 staining, and highest γ-H2AX and caspase-3 staining. Serum biochemical values were lower with L-Lip@DDP than with free cisplatin at corresponding temperatures, although values tended to rise with increasing perfusion temperature.

Conclusions

The tested sequential regimen showed favorable antitumor and biochemical findings with liposomal cisplatin, particularly at a nominal perfusion temperature of 43°C. These observations support a preclinical association among treatment conditions, tumor platinum accumulation, and response.

Background

Peritoneal dissemination and ascites are important manifestations of advanced ovarian cancer. Cytoreductive surgery and platinum-based systemic chemotherapy remain central components of treatment, and regional approaches have been investigated to improve disease control [1, 2]. For cisplatin, therapeutic use is constrained by renal toxicity, which varies with patient characteristics and

supportive treatment [3, 4]. Strategies that alter tumor platinum exposure while limiting adverse effects therefore warrant pharmacological evaluation.

Hyperthermic intraperitoneal chemotherapy (HIPEC) combines intraperitoneal administration of a cytotoxic drug with regional heating during surgery. OVHIPEC-1 demonstrated benefit in selected patients undergoing interval cytoreductive surgery after neoadjuvant chemotherapy [1, 2]. CHIPOR evaluated cisplatin-based HIPEC in selected patients with recurrent ovarian cancer [5], whereas a randomized phase II study of carboplatin HIPEC during secondary cytoreduction did not show superior clinical outcomes [6]. These studies address specific surgical and pharmacological settings. Their findings cannot be directly transferred to heated saline perfusion followed by intravenous chemotherapy.

Liposomal formulations offer a means of modifying the distribution and biological effects of platinum-containing treatment. Recent experimental studies have evaluated cisplatin-containing liposomes in ovarian tumor models and other cancer systems [7–9]. These formulations differ in surface modification, cargo, release properties, and dosing, so their performance does not establish the behavior of another liposomal preparation. Comparative measurements of tumor platinum, antitumor response, and toxicity are required for the formulation and schedule under investigation.

Regional heating may also influence the disposition of subsequently administered nanocarriers. In window-chamber tumor models, local hyperthermia increased liposome extravasation, with effects that persisted after heating [10, 11]. This provides a biological rationale for examining sequential heating and drug administration. However, the thermal exposures in those studies differ from a 15-min intraperitoneal perfusion, and they do not validate a 30-min post-perfusion dosing interval in the ID8 model. In the present work, thermal priming describes the treatment sequence and does not imply that a persistent vascular change has been demonstrated.

We evaluated intraperitoneal saline perfusion at four nominal temperatures followed by intravenous L-Lip@DDP or free cisplatin in mice bearing ID8-Luc peritoneal tumors. Following model establishment and characterization of the formulation and treatment procedure, we examined optical distribution, tumor platinum accumulation, and temperature-dependent cell-associated fluorescence. Ascites, representative tumor findings, immunohistochemical markers, and preliminary toxicity-related endpoints were then evaluated. These measurements were used to describe the pharmacological response to the tested regimen without assuming a causal delivery mechanism.

Methods

Study design

This preclinical study compared intravenous free cisplatin (free DDP) and liposomal cisplatin (L-Lip@DDP) after intraperitoneal normal-saline perfusion at nominal temperatures of 37, 41, 43, or 45°C. The 37°C condition served as the normothermic perfusion comparator. Model development was

evaluated over 21 days, followed by a 3-week treatment period. Tumor-bearing mice were randomly allocated to the temperature–formulation groups.

Cell culture and establishment of the animal model

Female C57BL/6 mice aged 4–6 weeks and weighing 16–20 g were purchased from Beijing Vital River Laboratory Animal Technology Co., Ltd. Each mouse received an intraperitoneal inoculation of 5×10^6 luciferase-expressing ID8 ovarian cancer cells (ID8-Luc). Tumors were allowed to develop for 3 weeks. Model development was evaluated by serial abdominal circumference measurements in five independent mice, bioluminescence imaging on days 7, 14, and 21, and representative gross examination (Fig. 1). The specimens illustrated in Fig. 1D were collected in July 2026.

Parental ID8 cells were obtained from the Cell Bank of the Chinese Academy of Sciences. The laboratory-established ID8-Luc cell line was generated using Lenti-CMV-firefly Luciferase-puro (GeneChem, Shanghai, China), followed by puromycin selection. Cells were cultured in high-glucose DMEM (Gibco) supplemented with 10% fetal bovine serum (Gibco), 100 U/mL penicillin, and 100 μg/mL streptomycin at 37°C in a humidified atmosphere containing 5% CO_2.

Cisplatin formulation and nanoparticle characterization

Free cisplatin (free DDP) and the liposomal cisplatin preparation L-Lip@DDP were evaluated. Nanoparticle morphology was examined using a JEOL JEM-2100 transmission electron microscope, and particle-size distribution was measured by dynamic light scattering using a Malvern Zetasizer Nano ZS analyzer (Fig. 2A).

Materials used in the established laboratory formulation workflow included cisplatin, egg-yolk phosphatidylcholine (Aobox Biotechnology, Beijing, China), cholesterol (Sigma–Aldrich), and lipopolysaccharide (Solarbio, Beijing, China). The liposomal preparation was based on the laboratory thin-film hydration procedure. The designation L-Lip@DDP is used throughout this manuscript for the cisplatin formulation evaluated in the present experiments.

Intraperitoneal perfusion and intravenous treatment

Tumor-bearing mice underwent intraperitoneal normal-saline perfusion under isoflurane anesthesia using a system supplied by Chongqing Ronghai Chaosheng Yixue Gongcheng Yanjiu Zhongxin Youxian Gongsi (Chongqing, China). The nominal perfusion temperatures were 37, 41, 43, and 45°C. Intraperitoneal temperature was monitored using an animal temperature probe, and the 15-min perfusion interval began after the target intraperitoneal temperature had been reached (Fig. 2D). Free DDP or L-Lip@DDP was administered by tail-vein injection 30 min after perfusion completion. This sequential treatment was repeated three times weekly for 3 weeks (Fig. 2B,C). The saline perfusate contained no

cisplatin. Temperature labels refer to nominal perfusion conditions unless measured intraperitoneal temperature is explicitly stated.

Free DDP and L-Lip@DDP were each administered at 2 mg/kg cisplatin equivalents per injection.

Bioluminescence and fluorescence imaging

Bioluminescence imaging was used to monitor ID8-Luc tumor development (Fig. 1C). Fluorescence imaging of the Nile Red-labeled preparation was performed at 6 and 12 h after tail-vein injection using an IVIS Spectrum imaging system (PerkinElmer; Fig. 3A). Nile Red was obtained from Shanghai Yuanye Bio-Technology. Fluorescence was acquired at excitation/emission wavelengths of 560/630 nm, with consistent exposure and gain settings across the compared samples. In vivo and ex vivo images were evaluated separately from the luciferase-dependent bioluminescence images.

Tumor platinum determination

Tumor nodules were collected after completion of treatment from five mice per group. Excised nodules were weighed and digested in concentrated aqua regia at 90–120°C until the solutions became clear. Digests were diluted with deionized water, and platinum content was determined by inductively coupled plasma optical emission spectrometry (ICP-OES; Agilent 5110). Platinum measurements were normalized to tissue weight and expressed as μg Pt/g tissue (Fig. 3B). This assay measured total tissue platinum separately from fluorescence distribution.

Cellular fluorescence assessment

ID8 cells were exposed to the Nile Red-labeled preparation at 37, 41, 43, or 45°C. DAPI (Beyotime, Shanghai, China) was used to identify nuclei, and cell-associated red fluorescence was observed using an inverted fluorescence microscope (Fig. 3C). Fluorescent foci were counted on a per-cell basis (Fig. 3D), with each heated condition compared with 37°C. This endpoint represented cell-associated label fluorescence rather than a direct measurement of intracellular platinum.

Ascites and gross tumor assessment

Ascitic fluid was collected and its volume measured at the treatment-evaluation endpoint (Fig. 4A). Representative abdominal dissections were photographed to document visible peritoneal nodules. The tumor H&E sections in Fig. 4B were obtained from the corresponding free-DDP and L-Lip@DDP groups at 45°C. These sections were used to illustrate tumor morphology and were not treated as a histological comparison across all temperatures.

Tumor immunohistochemistry

Tumor tissues were fixed in 4% paraformaldehyde, embedded in paraffin, and sectioned at 4 μm. Sections were deparaffinized in xylene, rehydrated through graded ethanol, and subjected to heat-induced antigen retrieval. Endogenous peroxidase activity was blocked using 3% hydrogen peroxide for 10–15 min. After protein blocking, sections were incubated overnight at 4°C with antibodies against Ki-67 (Abcam, ab16667), γ-H2AX (Cell Signaling Technology, 9718S), or caspase-3 (Cell Signaling Technology, 9662S). Sections were washed with PBS, incubated with horseradish-peroxidase-conjugated secondary antibodies, developed with diaminobenzidine, and counterstained with hematoxylin. Images were acquired by light microscopy (Fig. 5A,B). Relative staining levels were compared between 41, 43, or 45°C and the corresponding 37°C condition separately within each formulation (Fig. 5C).

Body weight and serum biochemical assessment

Body weight was monitored using an animal weighing scale during the observation period (Fig. 6A). Blood was collected at the experimental endpoint, and serum was separated by centrifugation for biochemical analysis. Serum alkaline phosphatase (ALP), aspartate aminotransferase (AST), blood urea nitrogen (BUN), and creatinine (CREA) were measured to assess treatment-associated changes in hepatic and renal biochemical markers (Fig. 6B).

Histological assessment of tumors and organs

Tumor nodules and the intestine, heart, liver, spleen, lung, and kidney were fixed in 4% paraformaldehyde, paraffin-embedded, and cut into 4-μm sections. Sections were deparaffinized in xylene, rehydrated through graded ethanol, stained with hematoxylin, differentiated and blued, and counterstained with eosin. After dehydration and clearing, sections were mounted and examined by light microscopy. Representative images were used to assess tumor morphology and visible injury-related changes in the organs (Figs. 4B and 6C,D).

Animal euthanasia:

At the experimental endpoint, mice were euthanized by carbon dioxide (CO_2) inhalation without prior administration of an anesthetic. CO_2 was introduced gradually at a displacement rate of 50% of the chamber volume per minute. The total duration of CO_2 administration was 20 min, with gas flow maintained for at least 1 min after respiratory arrest. Death was confirmed by the absence of spontaneous breathing and heartbeat before tissue collection.

Statistical analysis

Data are presented as mean ± standard deviation (SD). Statistical significance among multiple groups was evaluated using one-way ANOVA. All statistical analyses were performed using SPSS 22.0 software, and $P < 0.05$ was considered statistically significant

Results

Development of the ID8-Luc peritoneal dissemination model

Serial abdominal circumference measurements increased during the 21-day model-development period (Fig. 1A,B). Representative bioluminescence images showed increasing abdominal signal intensity and extent between days 7 and 21 (Fig. 1C). Gross examination demonstrated abdominal distension, peritoneal nodules and blood-tinged ascitic fluid (Fig. 1D). These observations supported establishment of a model with peritoneal tumor dissemination and ascites.

Formulation characterization and sequential treatment procedure

TEM showed approximately rounded particles, and the particle-size measurement was 52.74 ± 64.42 nm (Fig. 2A). The treatment schedule comprised three weekly treatments over 3 weeks (Fig. 2B). Each procedure separated 15-min saline perfusion from intravenous drug administration by a 30-min post-perfusion interval (Fig. 2C). The measured intraperitoneal temperature profiles showed heating, a plateau, and cooling, with distinguishable profiles for the nominal 37, 41, 43, and 45°C conditions (Fig. 2D). These measurements characterize the tested formulation and thermal procedure; they do not demonstrate temperature-triggered drug release.

Drug distribution and cellular fluorescence

Representative ex vivo and in vivo optical images were obtained at 6 and 12 h after tail-vein injection (Fig. 3A). The images showed liver-associated signal at 6 h and signal associated with peritoneal tumor nodules at 12 h. These findings describe the displayed distribution qualitatively.

Tumor platinum content was higher with L-Lip@DDP than with free DDP at each tested temperature, corresponding to the within-temperature comparisons indicated in Fig. 3B. For both formulations, the highest plotted tumor platinum content occurred at 43°C. Because the annotated comparisons address formulation differences within temperature groups, the temperature-related pattern is described as an observed trend rather than a demonstrated between-temperature statistical effect.

In the separate cell experiment, ID8 cells showed L-Lip@DDP-associated red fluorescence in the cellular regions surrounding DAPI-stained nuclei (Fig. 3C). Quantification of the corresponding fluorescent foci per cell showed higher counts at 41, 43, and 45°C than at 37°C, with the largest plotted counts at 43°C (Fig. 3D). Counts at 45°C were lower than those at 43°C, although the annotated comparisons were against 37°C.

Ascites formation and gross peritoneal tumor findings

Ascites volume was lower in the L-Lip@DDP groups than in the free-DDP groups across the tested temperatures. Within both formulations, the plotted volume decreased from 37 to 43°C and increased again at 45°C. The lowest plotted ascites volume occurred in the L-Lip@DDP group at 43°C (Fig. 4A). The

across-temperature pattern is described qualitatively. Representative dissections showed differences in visible peritoneal nodules across treatment conditions, with fewer conspicuous nodules in the L-Lip@DDP image at 43°C (Fig. 4B). These gross findings were not used as a quantitative nodule-count endpoint. The accompanying H&E images provided representative tumor morphology, rather than a histological comparison covering all temperatures.

Tumor immunohistochemical responses across treatment temperatures

Representative tumor sections and their relative staining measurements showed lower Ki-67 staining in the heated groups than at 37°C within each formulation (Fig. 5A–C). The lowest plotted Ki-67 level occurred at 43°C. γ-H2AX and caspase-3 staining increased in the heated groups, with the highest plotted values at 43°C and lower values at 45°C (Fig. 5C). Statistical annotations compare each heated condition with the corresponding 37°C group separately for L-Lip@DDP and free DDP.

Body weight and organ safety assessments

Both displayed body-weight curves increased over the observation period, and the marked comparison was labeled not significant (Fig. 6A). ALP, AST, BUN, and CREA values were lower in L-Lip@DDP groups than in free-DDP groups at corresponding temperatures, as indicated by the within-temperature comparisons in Fig. 6B. Values tended to increase with perfusion temperature in both formulations and were highest at 45°C. Between-temperature statistical comparisons were not indicated in this panel.

Representative intestinal and major-organ H&E images are shown in Fig. 6C,D. Without quantitative injury scoring and a healthy reference group in the displayed results, these sections provide descriptive morphological information. The lower biochemical values with L-Lip@DDP support a relative difference between treatment groups, but they do not establish normal organ function, absence of injury, or comprehensive systemic safety.

Discussion

This study evaluated intraperitoneal saline perfusion followed by intravenous cisplatin formulations in a mouse model of ovarian cancer peritoneal dissemination. After model verification and characterization of the formulation and perfusion procedure, the distribution-related findings showed higher tumor platinum content with L-Lip@DDP than with free DDP at corresponding temperatures. The separate cell experiment showed temperature-dependent formulation-associated fluorescence. These observations were accompanied by lower ascites volumes, temperature-related tumor staining patterns, and lower biochemical values with L-Lip@DDP. A nominal temperature of 43°C gave the most favorable observed combination of tumor platinum, cellular foci, ascites, and tumor staining among the tested conditions. The findings support further pharmacological evaluation of the sequential regimen without establishing a causal link between distribution and antitumor response.

The distinction from clinical HIPEC is fundamental to interpreting the study. HIPEC trials evaluate heated intraperitoneal chemotherapy in defined surgical settings [1, 2, 5, 6], and a randomized translational study has examined the effects of heat on cisplatin penetration during intraperitoneal treatment [12]. Our perfusate contained saline, and cisplatin was delivered intravenously after heating had ended. The present animal experiment therefore addresses the effect of preceding regional thermal exposure on a systemic drug regimen. It does not test a replacement for surgical HIPEC, compare clinical treatment standards, or establish that repeated saline perfusion is feasible or beneficial in patients.

Administering drug 30 min after perfusion provides temporal separation between the thermal procedure and drug delivery. Persistent effects of heating offer a plausible rationale for examining this sequence. Kong and colleagues observed post-heating liposome extravasation in a SKOV-3 window-chamber model, and Li and colleagues demonstrated sustained permeability changes following local hyperthermia in other tumor models [10, 11]. However, those studies used different heating durations, anatomical settings, and carrier systems. The present 15-min perfusion and 30-min interval were tested as one schedule, not established as an optimum. Without measurements at the time of injection, persistence of a vascular effect in the current model remains hypothetical.

Tumor platinum measurement is a direct tissue-level endpoint, but its interpretation has limits. Higher total platinum with L-Lip@DDP (Fig. 3B) may reflect altered circulation, retention, release, uptake, or clearance. It cannot distinguish intact liposomes from released platinum species or establish that more active cisplatin reached tumor-cell DNA. The liver-associated and tumor-nodule-associated optical signals in Fig. 3A provide qualitative spatial observations, not a quantitative transfer of drug from liver to tumor. The cellular fluorescence findings in Fig. 3C,D are consistent with a temperature-related change in cell-associated signal, but do not establish the source of the tumor platinum difference in vivo. Together, these measurements are compatible with a delivery-related effect while leaving the responsible process unresolved. Results from other cisplatin-containing liposomes illustrate the importance of formulation-specific pharmacology rather than proving the mechanism of L-Lip@DDP [7–9].

The temperature pattern also requires restrained interpretation. The plotted ascites, cellular-foci and staining measures were most favorable at 43°C (Figs. 3D, 4A and 5C), while increasing nominal temperature to 45°C did not improve these observations. This suggests that greater heating does not necessarily yield a greater response in the tested system. It does not establish a clinically usable thermal window, because nominal perfusate temperature is not a complete measure of tumor thermal dose and the study did not optimize heating duration or dosing interval. In particular, the within-temperature formulation comparisons in the platinum panel do not demonstrate that heating selectively benefits the liposomal formulation more than free drug. Such a claim would require an appropriate interaction analysis of the existing data.

The immunohistochemical findings (Fig. 5) provide complementary information about tumor response after assessment of ascites and gross peritoneal findings (Fig. 4). Lower Ki-67 staining is consistent with reduced proliferative activity, while increased γ-H2AX staining is consistent with a DNA-damage

response [13]. Neither marker proves that the observed response was mediated by increased platinum delivery. Heat can affect DNA-repair biology in other experimental systems [14], but no specific repair pathway was tested here. The caspase-3 antibody recognizes full-length protein as well as cleavage products. Consequently, increased immunoreactivity does not establish an increased apoptotic-cell fraction. The cellular fluorescence experiment provides a separate temperature-dependent observation and does not establish the in vivo delivery mechanism.

The biochemical results (Fig. 6B) favor L-Lip@DDP relative to free DDP under the tested conditions. This comparison is relevant because renal toxicity remains a major concern in cisplatin treatment and is influenced by dosing and supportive care [3, 4]. Nevertheless, lower CREA, BUN, AST and ALP values do not alone show that the values were normal, that renal platinum exposure was lower, or that tissue injury was absent. Both formulations showed higher plotted biochemical values at greater perfusion temperatures. Representative organ sections cannot establish an absence of toxicity without standardized assessment and appropriate reference groups. Body-weight gain is also difficult to interpret in an ascites-bearing model because fluid accumulation can affect weight independently of general health.

Several limitations define the scope of the conclusions. The study used one tumor model and a fixed treatment schedule. No saline-perfusion-only, untreated, or healthy reference results are included, limiting separation of heat effects, drug effects and disease-related changes. Vascular permeability, blood flow, intact-carrier localization, temperature-dependent drug release and comprehensive pharmacokinetics were not measured. The presented fluorescence observations cannot substitute for those measurements. Survival and recurrence were not assessed. Finally, repeated intraperitoneal access and the differences between murine and human abdominal heating limit direct clinical extrapolation. The findings are therefore best interpreted as associations between the tested treatment conditions, tissue platinum and measured responses, rather than proof of a vascular mechanism or clinical superiority.

Conclusions

Intraperitoneal saline perfusion followed by intravenous L-Lip@DDP showed favorable ascites, tumor platinum and biochemical findings relative to free cisplatin in the tested mouse model. A nominal perfusion temperature of 43°C yielded the most favorable observed response pattern among the tested conditions. The study supports preclinical evaluation of this sequential regimen, while its mechanism, optimal timing and clinical applicability remain unestablished.

Abbreviations

ALP
alkaline phosphatase
AST

aspartate aminotransferase
BUN
blood urea nitrogen
CREA
creatinine
DAPI
4',6-diamidino-2-phenylindole
DDP
cisplatin
DLS
dynamic light scattering
H&E
hematoxylin and eosin
HIPEC
hyperthermic intraperitoneal chemotherapy
ICP-OES
inductively coupled plasma optical emission spectrometry
ID8-Luc
luciferase-expressing ID8 cells
L-Lip@DDP
the liposomal cisplatin formulation used in this study
Pt
platinum
SD
standard deviation
TEM
transmission electron microscopy.

Declarations

Ethics approval and consent to participate

All experimental procedures were performed humanely and in compliance with the guidelines approved by the Experimental Animal Ethics Committee of the China-Japan Friendship Hospital.

Consent for publication

Not applicable.

Competing interests

The authors declare that they have no competing interests.

Funding

This work was financially supported by the National Natural Science Foundation of China (82374227 and 82472653), the Capital's Funds for Health Improvement and Research (2024-2-40612), and the China-Japan Friendship Hospital Funds (2017-RC-4).

Author Contribution

Shiyu Zhang: Writing – original draft, Methodology, Formal analysis, Data curation. Chang Zhou: Investigation, Formal analysis, Data curation. Caiyao Chen: Investigation, Methodology. Bin Ling and Jing Liang: Writing – review & editing, Funding acquisition, Conceptualization, Supervision.

Acknowledgements

Not applicable.

Data Availability

The underlying data supporting the findings of this study are available from Shiyu Zhang (18636646337@163.com) on reasonable request.

References

1. van Driel WJ, Koole SN, Sikorska K, van Schagen JH, Schreuder HWR, Hermans RHM, et al. Hyperthermic Intraperitoneal Chemotherapy in Ovarian Cancer. N Engl J Med. 2018;378(3):230–40. 10.1056/NEJMoa1708618.
2. Aronson SL, Lopez-Yurda M, Koole SN, van Schagen JH, Schreuder HWR, Hermans RHM, et al. Cytoreductive surgery with or without hyperthermic intraperitoneal chemotherapy in patients with advanced ovarian cancer (OVHIPEC-1): final survival analysis of a randomised, controlled, phase 3 trial. Lancet Oncol. 2023;24(10):1109–18. 10.1016/S1470-2045(23)00396-0.
3. Galfetti E, Cerutti A, Ghielmini M, Zucca E, Wannesson L. Risk factors for renal toxicity after inpatient cisplatin administration. BMC Pharmacol Toxicol. 2020;21(1):19. 10.1186/s40360-020-0398-3.
4. Oka T, Kimura T, Suzumura T, Yoshimoto N, Nakai T, Yamamoto N, et al. Magnesium supplementation and high volume hydration reduce the renal toxicity caused by cisplatin-based

chemotherapy in patients with lung cancer: a toxicity study. BMC Pharmacol Toxicol. 2014;15:70. 10.1186/2050-6511-15-70.

5. Classe JM, Meeus P, Hudry D, Wernert R, Quenet F, Marchal F, et al. Hyperthermic intraperitoneal chemotherapy for recurrent ovarian cancer (CHIPOR): a randomised, open-label, phase 3 trial. Lancet Oncol. 2024;25(12):1551–62. 10.1016/S1470-2045(24)00531-X.
6. Zivanovic O, Chi DS, Zhou Q, Iasonos A, Konner JA, Makker V, et al. Secondary Cytoreduction and Carboplatin Hyperthermic Intraperitoneal Chemotherapy for Platinum-Sensitive Recurrent Ovarian Cancer: An MSK Team Ovary Phase II Study. J Clin Oncol. 2021;39(23):2594–604. 10.1200/JCO.21.00605.
7. Zhu M, Jia J, Tang H, Xie Y, Lv Z, Bao H, et al. Antitumor Efficacy, Pharmacokinetics, and Toxicity Studies of Novel Estrogen Receptors Targeted PEGylated Liposomes Encapsulating Paclitaxel and Cisplatin in SKOV-3 Tumor-Bearing Nude Mice, ICR Mice, and SD Rats. Mol Pharm. 2025;22(7):3715–33. 10.1021/acs.molpharmaceut.4c01457.
8. Demirbolat GM, Cakirli E, Saglam AB, Sarigul-Ozbek S, Abas BI, Cevik O. pH-triggered liposomal strategy for cisplatin in lung cancer therapy. Sci Rep. 2025;15(1):36349. 10.1038/s41598-025-20144-0.
9. Awad MG, El-Shafiey SH, Ali RA, Abd El-Monem DD, Badawy AA, Al-Serwi RH, et al. Targeted liposomal nano-therapy combining anthocyanin and cisplatin reduces Ehrlich ascites carcinoma burden. Front Pharmacol. 2025;16:1659575. 10.3389/fphar.2025.1659575.
10. Kong G, Braun RD, Dewhirst MW. Characterization of the effect of hyperthermia on nanoparticle extravasation from tumor vasculature. Cancer Res. 2001;61(7):3027–32.
11. Li L, ten Hagen TLM, Bolkestein M, Gasselhuber A, Yatvin J, van Rhoon GC, et al. Improved intratumoral nanoparticle extravasation and penetration by mild hyperthermia. J Control Release. 2013;167(2):130–7. 10.1016/j.jconrel.2013.01.026.
12. Demuytere J, Carlier C, Van Helden T, Belza J, Vanhaecke F, Xie F, et al. Effects of hyperthermia on cisplatin tissue penetration and gene expression in peritoneal metastases: results from a randomized trial in ovarian cancer. Br J Surg. 2024;111(4):znae078. 10.1093/bjs/znae078.
13. Rogakou EP, Pilch DR, Orr AH, Ivanova VS, Bonner WM. DNA double-stranded breaks induce histone H2AX phosphorylation on serine 139. J Biol Chem. 1998;273(10):5858–68. 10.1074/jbc.273.10.5858.
14. Krawczyk PM, Eppink B, Essers J, Stap J, Rodermond H, Odijk H, et al. Mild hyperthermia inhibits homologous recombination, induces BRCA2 degradation, and sensitizes cancer cells to poly (ADP-ribose) polymerase-1 inhibition. Proc Natl Acad Sci U S A. 2011;108(24):9851–6. 10.1073/pnas.1101053108.

Figures

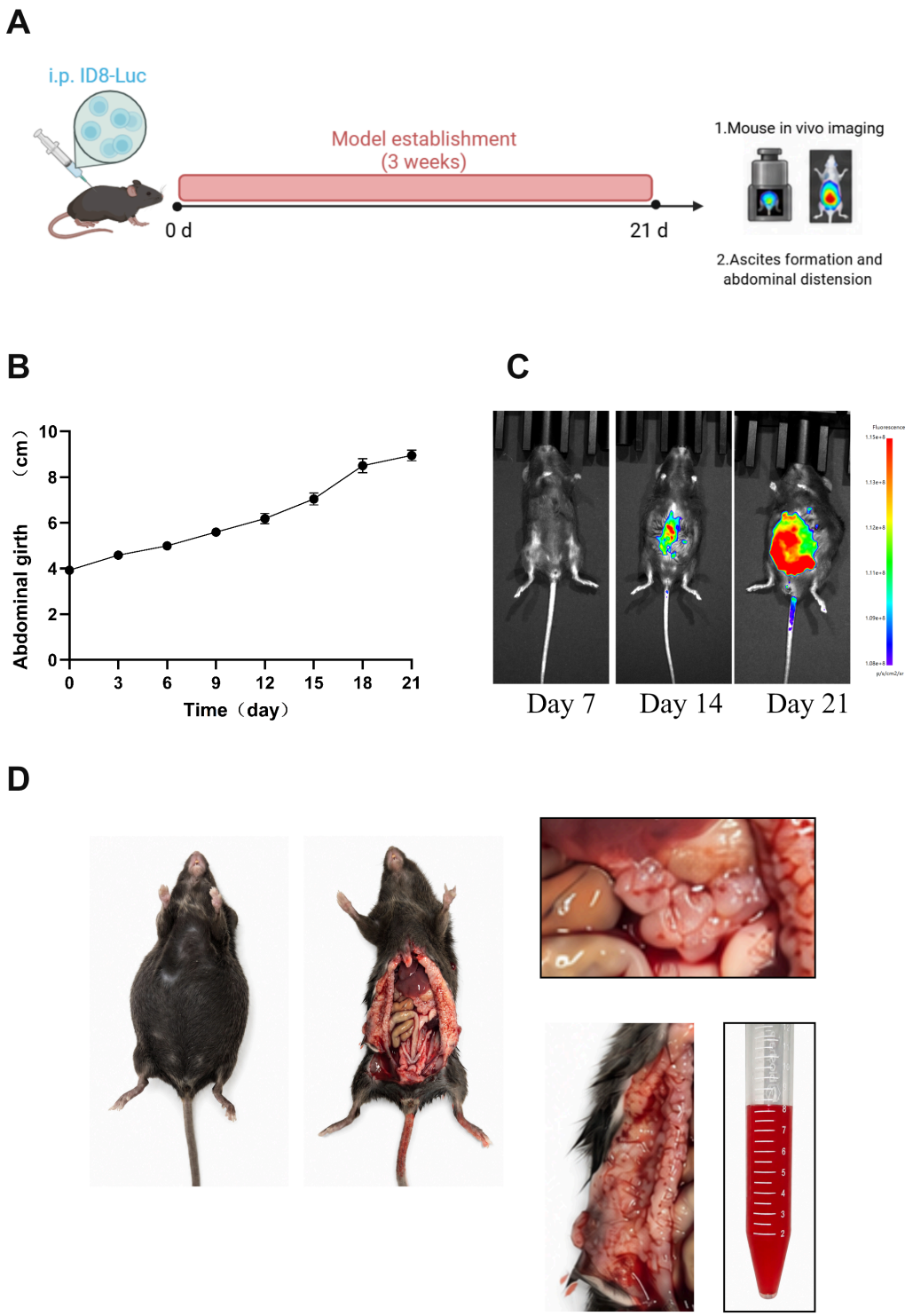

Figure 1

Establishment of the ID8-Luc peritoneal dissemination model

(A) Schematic of ID8-Luc cell inoculation, model development, and evaluation endpoints. (B) Serial abdominal circumference measurements during the 21-day model-development period; data are mean ± SD for five independent mice. (C) Representative in vivo bioluminescence images on days 7, 14, and 21.

(D) Representative gross appearance and dissection of tumor-bearing mice, showing abdominal distension, ascites, and disseminated nodules involving the peritoneum and intestinal surfaces; specimens were collected in July 2026. ID8-Luc, luciferase-expressing ID8 ovarian cancer cells.

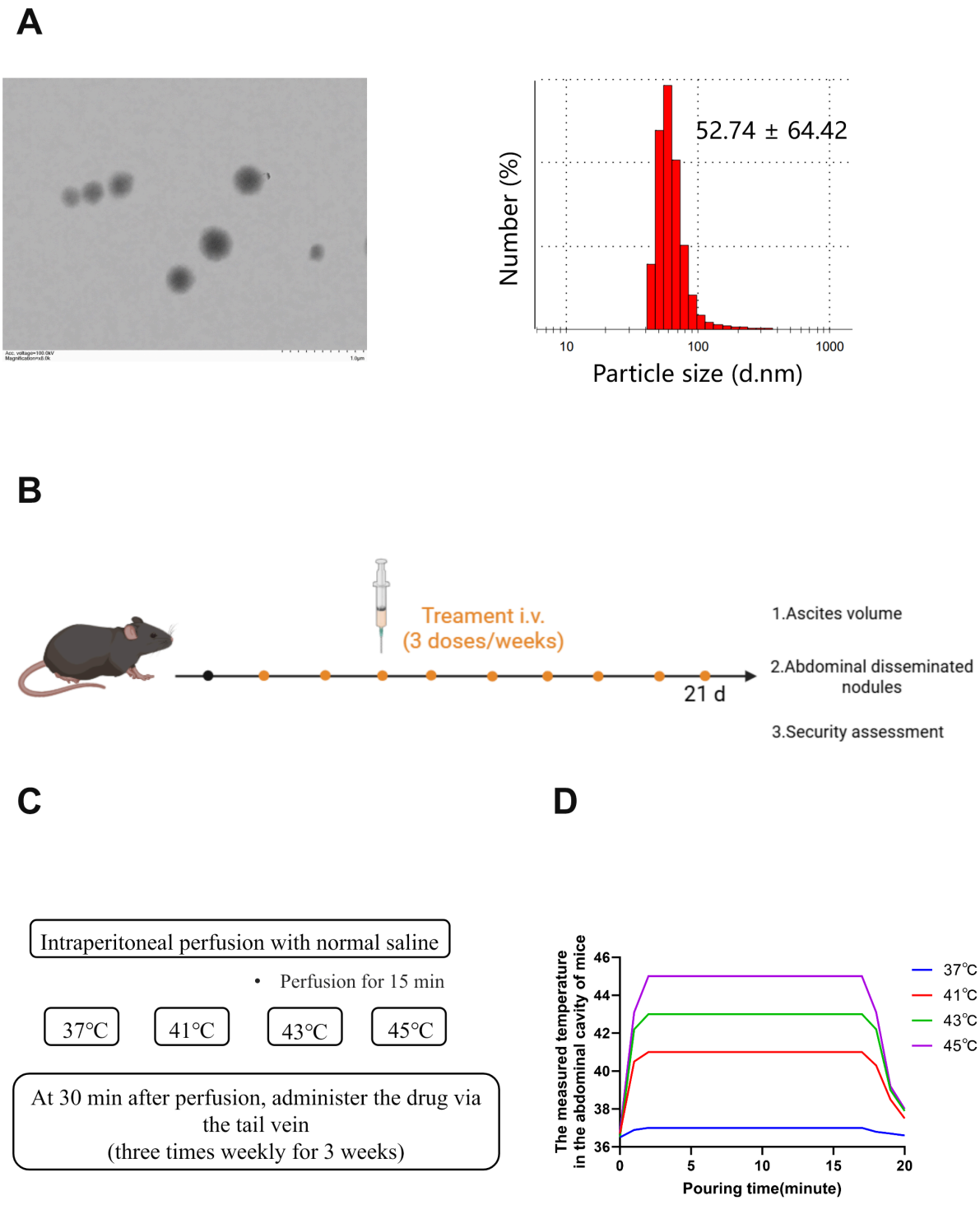

Figure 2

Formulation characterization and sequential perfusion and drug treatment

(A) Representative transmission electron microscopy (TEM) image and particle-size distribution of the liposomal formulation. (B) Treatment schedule and evaluation endpoints. (C) Intraperitoneal normal-saline perfusion at nominal temperatures of 37, 41, 43, or 45 °C for 15 min after the target intraperitoneal temperature was reached, followed 30 min after perfusion completion by tail-vein administration of L-Lip@DDP or free DDP at 2 mg/kg cisplatin equivalents. Treatment was repeated three times weekly for 3 weeks. (D) Measured intraperitoneal temperature over time during the procedure. DDP, cisplatin; L-Lip@DDP, liposomal cisplatin.

A

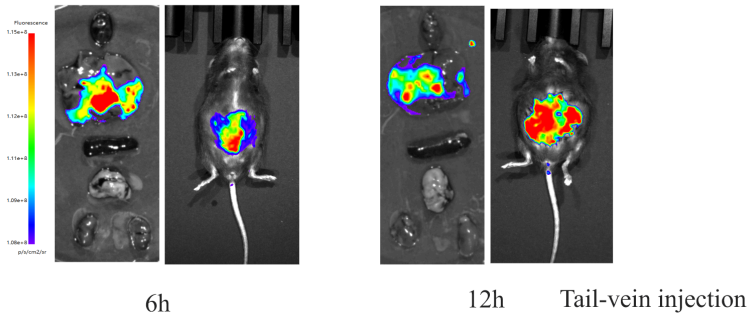

B

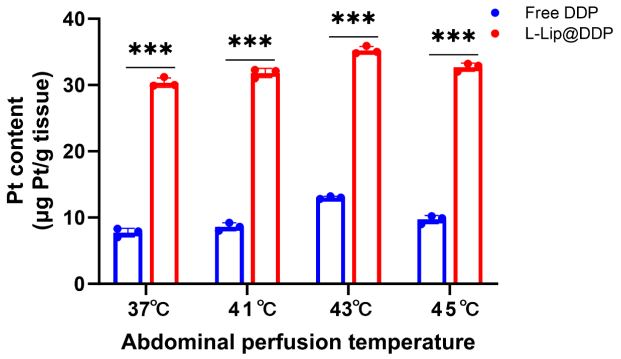

C

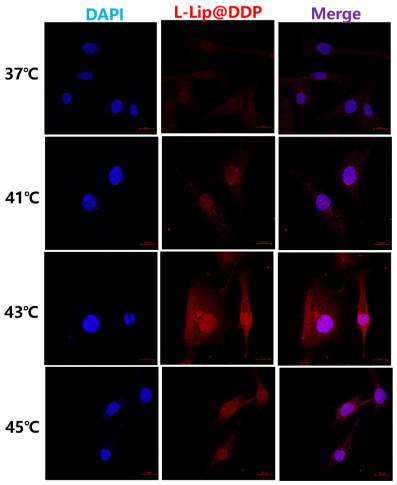

D

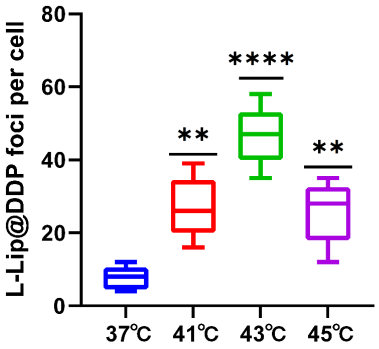

Figure 3

Optical distribution and tumor platinum accumulation and cellular uptake

(A) Representative ex vivo and in vivo fluorescence images of the Nile Red-labeled preparation at 6 and 12 h after tail-vein injection, showing liver-associated signal at 6 h and signal associated with peritoneal tumor nodules at 12 h. (B) Platinum content in tumor nodules collected after completion of treatment (n = 5 mice per group) at the indicated perfusion temperatures, expressed as μg Pt/g tissue; L-Lip@DDP and free DDP were compared within each temperature. Red, L-Lip@DDP; blue, free DDP. (C) Representative fluorescence images of ID8 cells at 37, 41, 43, and 45 °C. DAPI-stained nuclei are blue, formulation-associated fluorescence is red, and merged images are shown. (D) Fluorescent foci per cell corresponding to C; the 41, 43, and 45 °C conditions were each compared with 37 °C. Optical signals represent label-associated distribution and do not directly quantify platinum. **$P < 0.01$, ***$P < 0.001$, ****$P < 0.0001$.

A

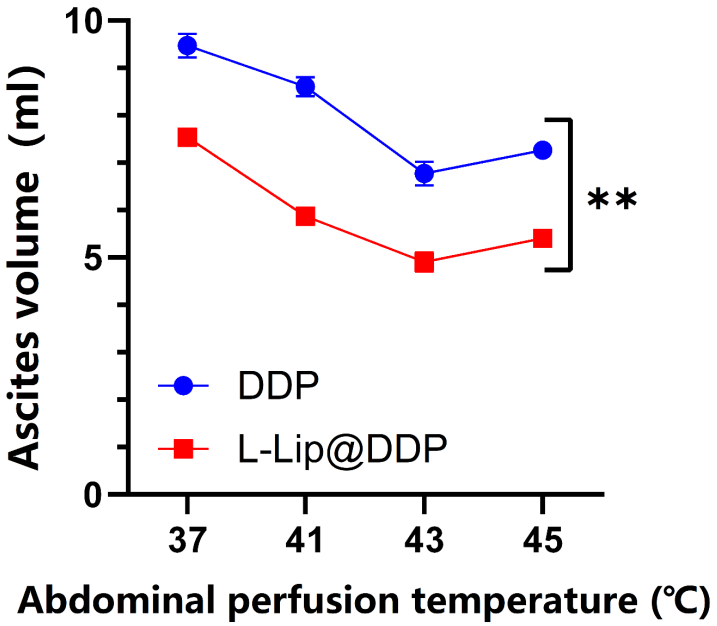

B

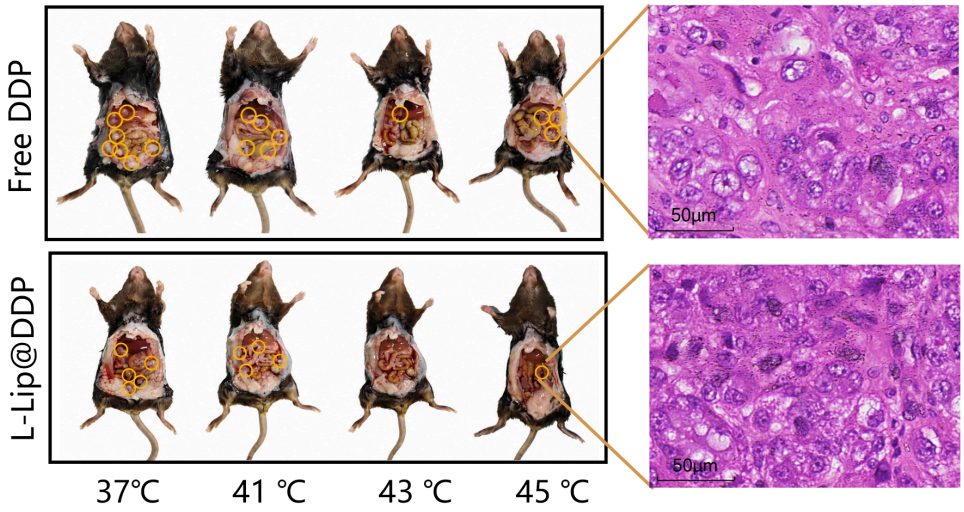

Figure 4

Ascites formation and gross peritoneal tumor findings

(A) Ascites volume in mice receiving L-Lip@DDP or free DDP after saline perfusion at the indicated temperatures. (B) Representative abdominal dissections showing peritoneal disseminated nodules (yellow circles), with representative H&E-stained tumor sections from the corresponding 45 °C groups.

Gross images are arranged by formulation and temperature, with free DDP in the upper row and L-Lip@DDP in the lower row. Scale bars in the H&E images, 50 μm. H&E, hematoxylin and eosin. **P < 0.01.

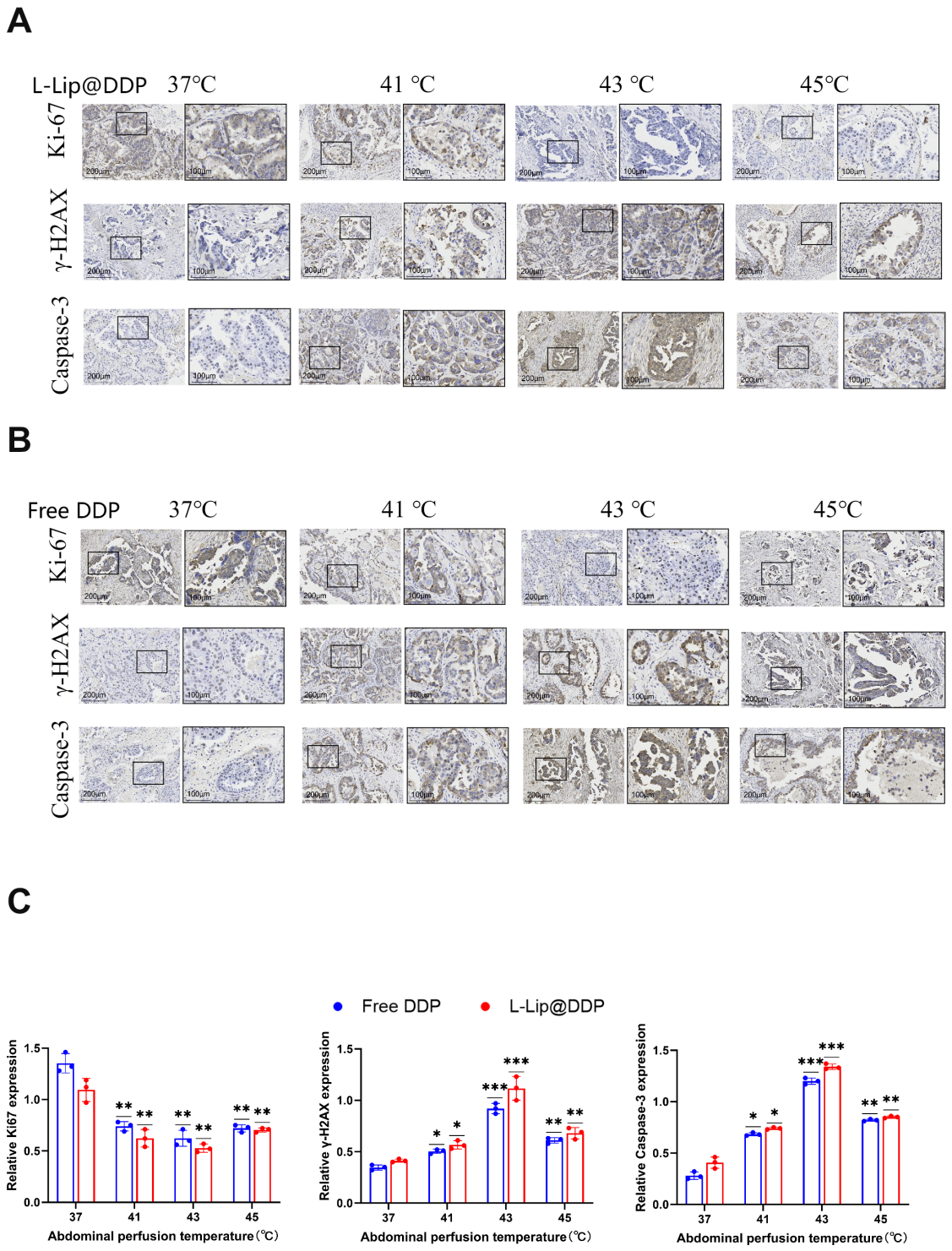

Figure 5

Tumor immunohistochemical responses across treatment temperatures

(A,B) Representative tumor sections from the L-Lip@DDP (A) and free-DDP (B) groups at nominal perfusion temperatures of 37, 41, 43, or 45 °C. Rows show Ki-67, γ-H2AX, and caspase-3 staining, with overview images and corresponding enlarged regions. Scale bars, 200 μm in overview images and 100 μm in enlarged images. (C) Relative staining levels of Ki-67, γ-H2AX, and caspase-3, from left to right. Red, L-Lip@DDP; blue, free DDP. Within each formulation separately, the 41, 43, and 45 °C groups were each compared with the corresponding 37 °C group. Symbols do not denote between-formulation comparisons. *P < 0.05, **P < 0.01, ***P < 0.001.

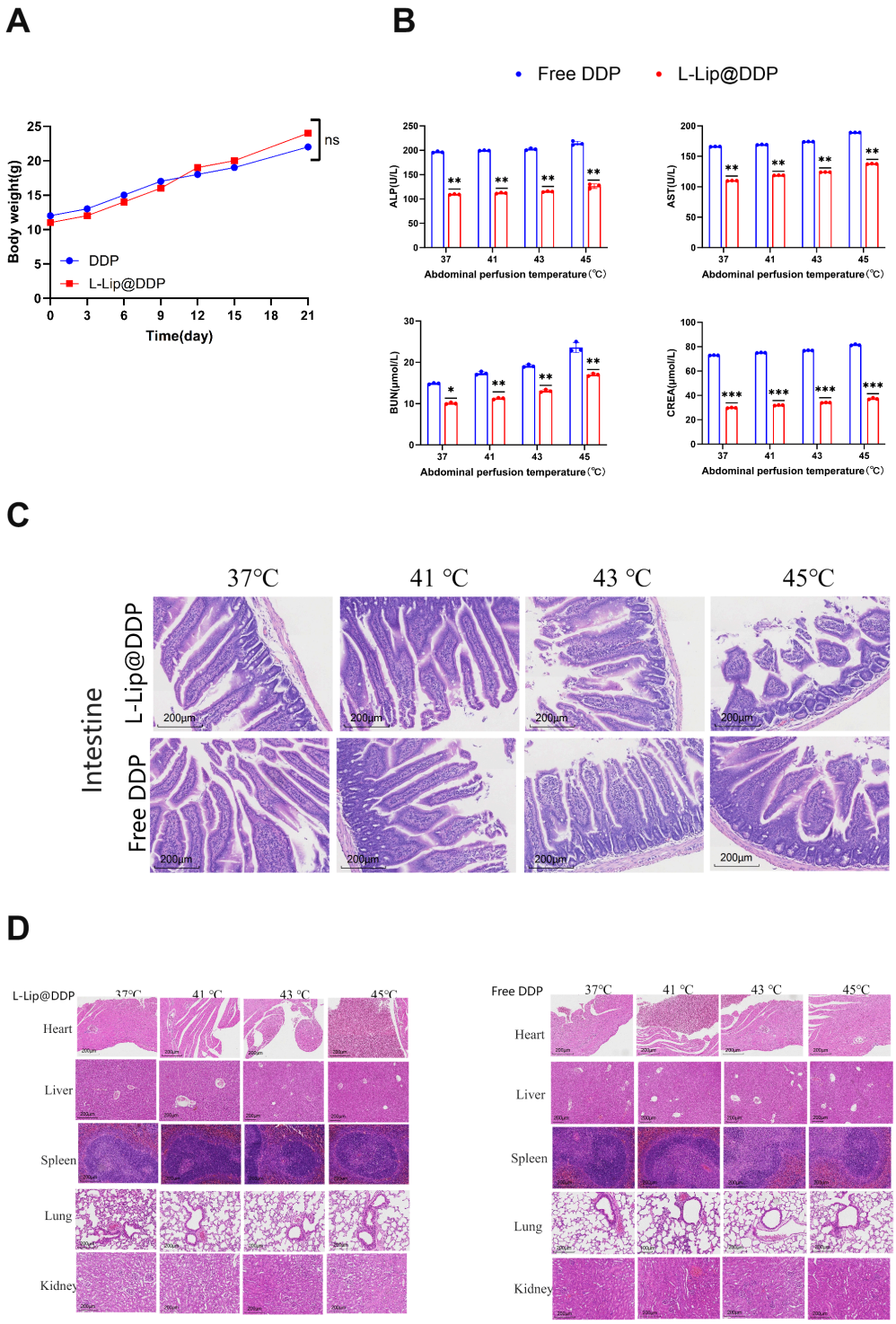

Figure 6

Body weight and serum biochemistry and tissue histology

(A) Body-weight measurements during the observation period. (B) Serum ALP (upper left), AST (upper right), BUN (lower left), and CREA (lower right) at the indicated perfusion temperatures. Red, L-Lip@DDP; blue, free DDP. Formulations were compared separately within each temperature for each marker. (C) Representative H&E-stained intestinal sections; L-Lip@DDP is shown above free DDP. (D) Representative H&E-stained heart, liver, spleen, lung, and kidney sections, from top to bottom; L-Lip@DDP is shown on the left and free DDP on the right, with temperature columns within each formulation. Scale bars in C and D, 200 μm. ALP, alkaline phosphatase; AST, aspartate aminotransferase; BUN, blood urea nitrogen; CREA, creatinine. *$P < 0.05$, **$P < 0.01$, ***$P < 0.001$; ns, not statistically significant.